How do quantum effects change conclusions about heterogeneous cluster behavior based on classical mechanics simulations?

Darryl J. Chartrand[a] and Robert J. Le Roy
Guelph-Waterloo Center for Graduate Work in Chemistry, University of Waterloo, Waterloo, Ontario N2L 3G1, Canada

(Received 8 August 1997; accepted 17 February 1998)

Comparisons of classical and quantum Monte Carlo simulation of SF_6–$(Ar)_n$ and SF_6–$(Ne)_n$ clusters are used to examine whether certain novel types of behavior seen in classical simulations of SF_6–$(Ar)_n$ and SF_6–$(Kr)_n$ persist when quantum effects are taken into account. For mixed clusters formed from Ar (and presumably other heavy partners) quantum effects have little effect on calculated properties, even at very low temperatures, so the cluster-size-dependent preference for solvation vs phase separation and ''reverse melting'' behavior found in the classical simulations may be expected to occur in many heterogeneous systems. On the other hand, quantum effects substantially lower the melting temperatures of clusters formed with Ne, and (except for a couple of unusually stable stacked isomers) effectively remove the barriers separating the maximally-solvated and phase-separated forms, implying that the latter will normally not exist. Moreover, for (at least) the SF_6–$(Ne)_{11}$ species, when quantum effects are taken into account there is little evidence of solidlike behavior down to the lowest temperatures accessible to our simulation (0.4 K), although classical simulations show a sharp freezing transition at $1.5(\pm 0.1)$ K. Inclusion of three-body triple–dipole Axilrod–Teller–Muto interactions in the overall potential energy has little effect on either quantum or classical Ne cluster simulations. © *1998 American Institute of Physics.* [S0021-9606(98)00620-5]

I. INTRODUCTION

The properties of molecular clusters have long been of theoretical interest because of their intermediate position between the isolated molecule and condensed phase domains, and because their finite size has made quantitative classical mechanical simulations feasible. Over the past decade or so, this interest has been heightened by the development of ever-improving experimental techniques for making such species and observing their properties.[1–5] In general, however, there has been only a modest degree of interaction between experiment and theory. Most theoretical work has focused on idealized homogeneous clusters of spherical atoms interacting through simple pairwise additive potentials, and on the calculation of collective ''theoretician's'' properties (such as potential energy or heat capacity) which are not amenable to direct measurement.[6–14] Such studies have contributed immensely to our qualitative understanding of the properties and types of behavior encountered in ''finite'' cluster systems, but the use of simple isotropic pairwise model potentials [usually LJ(12,6) functions] and neglect of both nonpairwise additive interactions and quantum effects make their quantitative implications uncertain.

In contrast, some of the most detailed experimental probing of the structure and properties of clusters has involved spectroscopic studies of nonspherical molecules in heterogeneous systems.[5,15–26] The present paper extends a line of theoretical work on such systems which uses the most realistic molecular interaction potentials available and showed that the perturbed infrared spectrum of a chromophore ''solute'' molecule inside of or attached to an inert gas ''solvent'' cluster can probe the structure and dynamical state of such systems.[27–38] That work focused attention on the family of clusters SF_6–$(Rg)_n$ (Rg=Ne, Ar or Kr), for which accurate Rg–Rg potential curves[39–41] and realistic anisotropic Rg–molecule potential surfaces[42,43] are known, and for which extensive experimental work has been done.[5,15–22,24–26] It showed that even for a quasispherical octahedral molecule like SF_6 interacting with rare gas ''solvent'' particles, the anisotropy of the pairwise potential can significantly affect proclivities for solvation or ''wetting'' vs phase separation in small clusters.[14,32,34]

Further work examined the effect of the three-body triple–dipole Axilrod–Teller–Muto (ATM) interactions[44,45] on conclusions regarding structural proclivities and melting behavior yielded by such simulations.[35] Barker and coworkers had shown that representing the total potential energy of a many-body system as a pairwise additive sum of the best available two-body potentials plus the ATM terms yielded predictions for the properties of bulk solid, liquid, and gaseous rare gas systems in very good agreement with experiment over a wide range of conditions.[46–51] This indicates that the triple–dipole dispersion energies provide a good effective representation of the overall nonadditive energy for such nonpolar species, albeit at least partly because of mutual cancellations of other types of nonadditive energies.[49,52–55] For heterogeneous SF_6–$(Ar)_n$ and SF_6–$(Kr)_n$ cluster systems, including such terms significantly affects the

[a]Present address: Department of Earth and Atmospheric Science, York University, North York, Ontario M3P 1J3, Canada.

melting temperatures determined from classical Monte Carlo and molecular dynamics simulations.[35] However, it did not change qualitative conclusions regarding trends in structural proclivities and melting behavior yielded by simulations based only on additive (anisotropic) two-body interactions.

Some of the most interesting results of these studies concerned the coexistence, persistence and different melting behavior of maximally-solvated (where the chromophore is surrounded by solvent atoms) vs phase-separated structural isomers of a given cluster.[30,32–34,56] For example, a novel ''reverse melting'' behavior was observed in classical molecular dynamics simulations of SF_6–$(Ar)_n$ $(n=7-12)$, where heating a maximally-solvated liquidlike structure allows it to isomerize into a solidlike phase-separated structure, where it lives for periods which are very long compared to the time scale of cluster vibrations.[30,32,56] In other words, *adding* energy to such clusters apparently allows a liquid to turn into a solid. Another intriguing result is the selective size-dependent solvation proclivities of these species, where the preference of the SF_6 for being maximally solvated vs phase separated varies with cluster size.[14,29,34] However, it is conceivable that the integrity of the distinct cluster isomers whose stable coexistence gives rise to these phenomena is an artifact of the fact that those simulations were based on classical mechanics. The present work examines this question for a variety of SF_6–$(Ar)_n$ and SF_6–$(Ne)_n$ clusters.

All of the early theoretical studies of the static and dynamical properties of clusters were based on classical Monte Carlo or molecular dynamics simulations. In the former, thermally averaged properties of the system are obtained by sampling the total configuration space in a stochastic manner, while in the latter the forces on each of the individual cluster components are calculated and the particles allowed to move according to Newton's equations of motion, and average values of properties are accumulated as the system evolves through real time. Use of these methods has greatly improved our general understanding of cluster behavior.[6–10,28,34,57,58] However, quantum effects become increasingly important both when the temperature is very low and for systems involving either very light species (such as He or H_2) or molecules with very small moments of inertia (such as the simple hydrides HF and CH_4), and quantum simulation methods have been extensively used for such cases.[36–38,59–61] Moreover, for small homogeneous clusters formed from atoms as heavy as Ne, quantum corrections have been shown to have significant effects on the melting temperatures.[62,63]

The present work extends the study of quantum effects in moderately heavy systems to heterogeneous clusters formed by SF_6 with Ne and Ar. In particular, the Fourier path integral Monte Carlo (PIMC) method is used to investigate the magnitude of quantum effects on their melting behavior, structural proclivities, and spectroscopic properties. Since the infrared spectral shifts of a solute or solvent chromophore have been found to be an incisive probe of the properties of such systems, the question of how these predicted spectra are influenced by introduction of quantum averaging is quite important. This study also examines the relative importance of quantum effects vs that of including nonadditive three-body forces in the description of the system. To this end, comparisons are made between properties calculated using the following four simulation methods: (1) classical Monte Carlo with only pairwise additive potentials, (2) Fourier path integral quantum Monte Carlo with only pairwise additive potentials, (3) classical Monte Carlo including triple–dipole ATM dispersion energies, and (4) Fourier path integral quantum Monte Carlo including triple–dipole dispersion energies.

In the following, Sec. II describes the potential energy surfaces used in this work, outlines the methodology, and presents illustrative convergence tests for our quantum PIMC simulations. Sections III and IV then present our results for clusters formed with solvent Ar and Ne atoms, respectively, while Sec. V summarizes our conclusions.

II. METHODOLOGY

A. The potential energy surface

In this work, the overall SF_6–$(Rg)_n$ potential energy function is defined as a sum of reliable two-body potentials for all pairs of species, and when included, the effects of many-body interactions are represented by the ATM triple–dipole dispersion energies.[44,45] For the latter case, the total potential for a set of n rare gas atoms located at positions $\{\mathbf{r}_i\}$ relative to an origin at the center of a single SF_6 molecule is therefore represented by the expression,

$$V(\mathbf{r_1},\mathbf{r_2},\ldots,\mathbf{r_n}) = \sum_{i=1}^{n} V_{\mathrm{Rg-SF_6}}(\mathbf{r}_i) + \sum_{i=1}^{n-1}\sum_{j>i}^{n} V_{\mathrm{Rg-Rg}}(r_{ij}) + \sum_{i=1}^{n-1}\sum_{j>i}^{n}\sum_{k>j}^{n+1} C_{ijk}[1+3\cos(\theta_i)\times\cos(\theta_j)\cos(\theta_k)]/(r_{ij}r_{jk}r_{ki})^3, \quad (1)$$

where $r_{ij}=|\mathbf{r}_{ij}|=|\mathbf{r}_i-\mathbf{r}_j|$, $\cos(\theta_i)=\mathbf{r}_{ki}\cdot\mathbf{r}_{ji}/r_{ki}r_{ji}$, C_{ijk} is the ATM triple–dipole dispersion coefficient for the three distinct particles i, j, and k, and particle number $k=n+1$ is the SF_6 molecule. Unlike some previous work in this area,[63,64] it was not found necessary to impose an artificial constraining potential in order to prevent cluster evaporation during a simulation run.

As in most previous studies of these systems,[27–35] the two-body potentials appearing in the first sum of Eq. (1) are represented by the full anisotropic Rg–SF_6 potentials of Pack *et al.*,[42,43] while those in the second sum are the accurate Rg–Rg interaction potentials of Aziz and Slaman.[39,40] Figure 1 compares these pair potentials for the three families of systems considered here; for each case, the solid curves show radial cuts through the anisotropic Rg–SF_6 potential energy surface along the three characteristic symmetry axes, while the dotted curve is the corresponding one-dimensional Rg–Rg potential. For all three systems, the anisotropy of the Rg–SF_6 potential is at least comparable to the overall strength of the Rg–Rg interaction. However, the Ne (and He) systems differ from the others in the greater weakness of the Rg–Rg interaction relative to both the anisotropy and the overall strength of the Rg–SF_6 potential; this has significant implications for their structural proclivities and dynamics.[34]

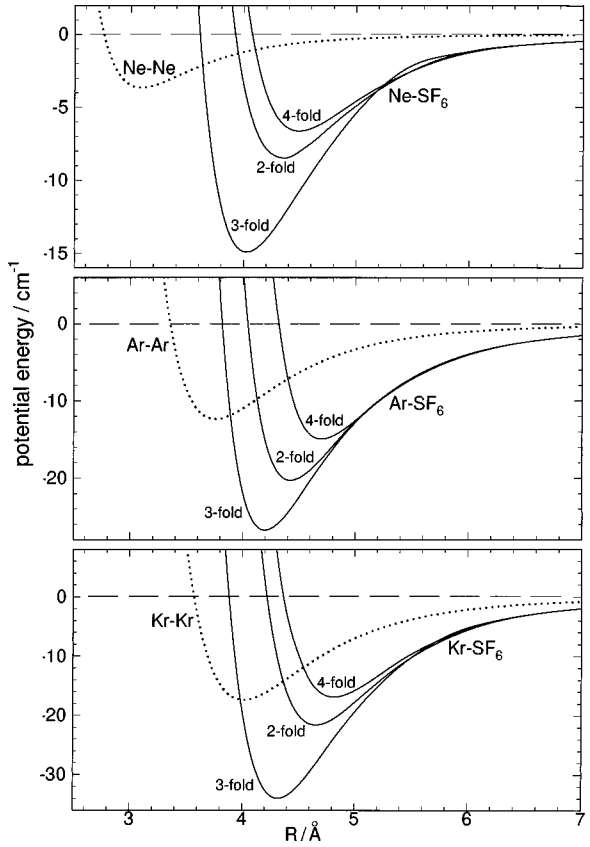

FIG. 1. Potential energy curves for a Rg=Kr, Ar or Ne atom approaching SF_6 (solid curves) along its characteristic two-, three-, and four-fold symmetry axes, and the associated one-dimensional Rg–Rg interaction potentials.

The triple–dipole dispersion energy coefficients C_{ijk} for both the $(Rg)_3$ and SF_6–$(Rg)_2$ species were calculated by Meath and co-workers, as described in previous papers.[35,65] For convenience, Table I summarizes their previously published values and their unpublished result[66] for SF_6–$(Ne)_2$.

B. Predicting the infrared spectra of SF_6–$(Rg)_n$ clusters

Eichenauer and Le Roy developed a model for predicting the spectral frequency shifts for IR active modes of a nonpolar chromophore molecule with polarizable nonpolar neighbors, and applied it to the fundamental band of the ν_3 mode of SF_6 in an SF_6–$(Rg)_n$ cluster.[29] This mode is a triply-degenerate asymmetric stretching vibration in which the sulfur atom vibrates along one of the three F–S–F axes while all of the fluorine atoms move in (approximately) the opposite direction. The presence of neighboring perturbing species tends to lift the degeneracy and shift the band center away from the free-monomer transition frequency. This model has been used with considerable success in explaining and interpreting the size and isomer-dependence of observed spectra in a variety of cases,[5,22,23,25,29,30,33,36,37] and is used to generate the synthetic spectra reported in the present work.

Within the above model,[29,31] the size of the overall band shift is approximately additive over the several rare gas atoms in the cluster, with the geometry of their particular arrangement about the SF_6 determining the pattern of the splitting into the three components.[33] For a given perturbing ''solvent'' particle, the magnitude of its contribution to the infrared spectral shifts is proportional to the product of the species' polarizability times $|\mathbf{r}_i|^{-6}$. Consequently, it is the solvent atoms in the first solvation shell which mainly determine the overall shift and the structure of the spectrum associated with a particular cluster configuration. The heterogeneously broadened thermal spectrum is then predicted by averaging these predicted shifts along the stochastic path of the Monte Carlo simulation.

It is important to realize that there are two distinct types of contributions to the overall width of the simulated spectra. The first is due to the lifting of the vibrational degeneracy by the asymmetry of the arrangement of neighboring perturbing species, and the second to the heterogeneous averaging along the stochastic path which broadens those component peaks. For liquidlike clusters, both effects are real and the simulated spectral shift distribution should provide realistic predictions of the overall line shape. However, for solidlike clusters (or quantum liquid clusters in or near their ground state[37]) the stochastic path broadening of the component peaks is an artifact of this simulation method, and the actual widths of the three component peaks may be much narrower than the simulation suggests. However, the pattern and magnitude of the splitting of the vibrational triplet should retain its significance as an indication of the asymmetry of the perturbing environment.

These arguments are consistent with the results of classical Monte Carlo simulations of the spectral shift distributions for SF_6 at various vacancy sites in an Ar lattice.[67] The overall shift and triplet splittings so obtained were comparable to those seen experimentally,[68] but the calculated distributions gave component peak widths much broader than those observed. This shows that for this matrix system the stochastic path averaging realistically samples the average chromophore environment, but it provides no estimate of the rate of the inhomogeneous processes which actually give rise to the observed broadening.

C. Melting criterion

One of the best ways to classify a cluster as being liquidlike or solidlike is through consideration of the temperature dependence of the relative root mean square bond length fluctuation parameter, $\delta(T)$. For m particles, labeled i or j with pairwise separations r_{ij}, this quantity is defined as

$$\delta(T)=\left[\frac{2}{m(m-1)}\right]\sum_{i=1}^{m-1}\sum_{j>i}^{m}\sqrt{\langle r_{ij}^2\rangle-\langle r_{ij}\rangle^2}/\langle r_{ij}\rangle, \qquad (2)$$

where $\langle p\rangle$ denotes the ensemble average value of property-p for the simulation of interest, the sums run over all distinct pairs of particles in the cluster, and the prefactor is the inverse of the number of distinct pairs in an m-particle cluster.

The so-called ''Lindemann criterion'' for melting was traditionally based on whether or not the calculated value of $\delta(T)$ was larger than some critical value such as 0.1.[7,8,10,57,58,69–72] However, since $\delta(T)$ tends to have distinctly different magnitudes in quantum and classical simulations (see below), it is more useful to focus on *trends* in its

behavior. In both quantum and classical simulations, $\delta(T)$ in the lowest temperature region tends to have relatively small values and to change very slowly. As T increases, however, it (usually) eventually undergoes a sharp rise over a narrow temperature range until it reaches some distinctly higher value where it plateaus, and then resumes a much slower growth rate with further increases in T. We associate the onset of this sharp rise with the melting of solidlike clusters.

Note that while Eq. (2) is written in terms of a sum over *all* particles in the cluster, for the heterogeneous systems considered here, where the Rg atoms often lie in a monolayer about the SF_6, the distances between those atoms and the SF_6 molecule tend to remain approximately constant, even when the Rg atoms have become highly mobile and are rearranging freely. In this case, a clearer indication of the onset of ''melting'' is obtained if one restricts the sums in Eq. (2) to involve only the Rg–Rg separations. To indicate the application of this restriction in most of the calculations reported herein, the values of $\delta(T)$ obtained in this way are denoted $\delta_{\mathrm{Rg-Rg}}$.

D. Path integral Monte Carlo simulations

Two techniques for taking account of quantum effects when calculating finite-temperature properties of many-body systems are the Fourier path integral Monte Carlo[73–75] and discretized path integral Monte Carlo methods.[76–78] They have been tested on and applied to a number of simple cluster systems.[62,64,73,74,76,79–81] These methods are essentially equivalent,[82] both involving an extension of classical Monte Carlo integration to take into account tunneling and zero point energy effects by the introduction of a more complex distribution function. The Fourier path integral method, which is used here, introduces an integration over an auxiliary spatial variable to examine and appropriately weight the region of configuration space surrounding each set of classical particle coordinates. Calculation of thermodynamic and other properties, such as infrared spectral shifts and root mean square bond length fluctuations, involves the same type of ensemble averaging as in the classical case, except that the averaging is done over an ''augmented'' coordinate space.[62,64,73,74,76,79–81]

In classical Monte Carlo simulations, the thermal average of a property p is calculated by evaluating integrals along the stochastic trajectory, weighting individual contributions by the Boltzmann distribution function $\exp(-\beta V)$,

$$\langle p\rangle = \frac{\int d\mathbf{R}\, \exp(-\beta V) p(\mathbf{R})}{\int d\mathbf{R}\, \exp(-\beta V)}. \tag{3}$$

Here, $\mathbf{R}$ is a multidimensional coordinate spanning all the spatial dimensions of the system, $V=V(\mathbf{R})$ is the total system potential energy, $\beta = 1/k_B T$, and k_B is Boltzmann's constant. Property-p is sampled periodically and summed over the length of the simulation.

In quantum statistical mechanics the expectation value of a property p which is diagonal in a coordinate representation can be evaluated using the expression,

$$\langle p\rangle = \frac{\int d\mathbf{R} p(\mathbf{R}) \langle \mathbf{R}|\exp(-\beta \widetilde{H})|\mathbf{R}\rangle}{\int d\mathbf{R} \langle \mathbf{R}|\exp(-\beta \widetilde{H})|\mathbf{R}\rangle}, \tag{4}$$

where $\widetilde{H}$ is the system Hamiltonian. This is similar to the classical average, except that it involves the diagonal density matrix elements $\langle \mathbf{R}|\exp(-\beta\widetilde{H})|\mathbf{R}\rangle$ instead of simply the classical Boltzmann weighting factor. This density matrix element can be represented by[73,74]

$$\langle \mathbf{R}|\exp(-\beta\widetilde{H})|\mathbf{R}\rangle = \int d\mathbf{R}(u) \exp\left[-\hbar^{-1} \int_0^{\beta\hbar} du \left(\frac{m\dot{\mathbf{R}}(u)^2}{2} + V(\mathbf{R}(u)) \right) \right], \tag{5}$$

where $\int d\mathbf{R}(u)$ implies an integration along all possible closed paths that start and end at $\mathbf{R}$. The expression in the exponent of the integrand of Eq. (5) has the generic form of a Feynmann action integral evaluated over the imaginary time $\beta\hbar$, where the parameter u measures ''time'' along this closed path.[83]

The Feynman action integrals of Eq. (5) can be evaluated by one of two equivalent methods.[82] The first is the discretized path integral Monte Carlo method, which essentially breaks the propagation along the path into several discrete intermediate states for the purpose of evaluating the diagonal density matrix elements.[84] The second is the Fourier path integral Monte Carlo method (hereafter called PIMC), which is the method used here. This approach parametrically expresses each of the paths needed for the integration in Eq. (5) in terms of an infinite Fourier sine series for each spatial coordinate,

$$x_i(u) = x_i + \sum_{k=1}^{\infty} a_{ki} \sin\left(\frac{k\pi u}{\beta\hbar} \right). \tag{6}$$

Summing over these various paths is effectively equivalent to summing over an ensemble of sets of randomly chosen Fourier coefficients (FC's) $\{a_{ki}\}$, which effectively ''smears'' out the classical end points or particle coordinates, so that the classical potential energy at a particular value of $\mathbf{R}$ is replaced by an effective potential associated with many-dimensional paths of the system which start and end at those same end points.[85] These FC's are sampled from a Gaussian distribution of variance,

$$\sigma_{ki} = \sqrt{2\beta\hbar^2/m_i(\pi k)^2}. \tag{7}$$

The net result is that one is able to express quantum mechanical equilibrium expectation values in the form of classical-like averages over an augmented configuration space.[86] As is indicated by Eq. (7), the range of probable values of the FC's associated with the spatial coordinates of a particle of mass m_i varies inversely as the product of the Fourier coefficient index k with the square root of the particle mass times the temperature. In practical calculations, the infinite sum in Eq. (6) is truncated at $k_{\max}$, the smallest number of terms for which the calculated properties converge to within some specified tolerance. The fact that one

can use different k_{max} values for different coordinates or particles in a given system is one of the (underexploited) advantages of this approach.

In a practical PIMC simulation for an m-particle system, the diagonal density matrix elements of Eq. (5) are represented by

$$\langle \mathbf{R}|\exp(-\beta\widetilde{H})|\mathbf{R}\rangle \approx \exp\left[-\sum_{k=1}^{k_{max}}\sum_{i=1}^{3m}\frac{a_{ki}^2}{2\sigma_{ki}^2} - \frac{1}{\hbar}\int_0^{\beta\hbar} V(\mathbf{R}(u))du\right], \quad (8)$$

where the first term in the exponent is the kinetic energy contribution to the ''action integral'' introduced in Eq. (5), which essentially is a sum over the FC's of all coordinates of the system, while the second term is an integral along the path from 0 to $\beta\hbar$ defined by that particular set of $\{a_{ki}\}$ coefficients.[73,74] This integral is easily evaluated using a Gaussian quadrature. The overall numerical methodology therefore involves the usual Monte Carlo random walk of all spatial coordinates of the system $\{x_i\}$, coupled with a simultaneous random walk over values of the $\{a_{ki}\}$ Fourier coefficients selected from Gaussian distributions of variance $\{\sigma_{ki}\}$, where for each set of $\{x_i, a_{ki}\}$ values one performs a Gaussian integration to evaluate the effective potential term in Eq. (8). The acceptance/rejection of a given move in $\{x_i, a_{ki}\}$ space is then based on the usual Monte Carlo criterion,[87,88] except that the classical weight function $\exp[-\beta V(\mathbf{R})]$ is replaced by the density matrix element of Eq. (8).

E. Numerical details and PIMC convergence tests

The convergence of calculated properties with respect to both the number of Fourier coefficients used, and the number of quadrature points for evaluating the integrals over $V(\mathbf{R})$ in Eq. (8), are critical questions in PIMC simulations. While the formal sum over the Fourier coefficients includes values of k from 1 to ∞, Eq. (7) shows that the length scale associated with the Fourier coefficients is inversely proportional to the index k. As a result, the oscillatory sine wave contributions to the fluctuations become less and less significant as the index become larger. In practice, one may simply include as many coefficients k_{max} as are needed to converge a calculated property to within some specified tolerance, an approach which is known as ''canonical PIMC.'' [80] However, the convergence of the results with respect to k_{max} can be very slow when the temperature of the system is low or the masses of the particles are small. To prevent convergence problems making such calculations prohibitively expensive, Coalson *et al.*[80] developed a technique called ''partial averaging,'' which has the effect of approximating the effects of higher order coefficients ($k > k_{max}$) without explicitly summing over them.

Tests of PIMC convergence with respect to k_{max} were performed for representative low temperature SF_6–$(Ar)_4$ and SF_6–$(Ne)_4$ clusters. Figure 2 shows how calculated values of $\langle V\rangle$ depend on k_{max} for simulations performed using both canonical PIMC and partial averaging; the associated uncertainties are all approximately 0.1 meV. These results were obtained using eight quadrature points to evaluate the potential energy integrals of Eq. (8). In analogous plots of δ_{Rg-Rg} vs k_{max}, the canonical and partially averaged results are very similar to one another, but their overall convergence behavior is quite similar to that for the partially averaged $\langle V\rangle$ results. For both of these systems the converged PIMC value of δ_{Rg-Rg} [of 0.042 for SF_6–$(Ar)_4$ and 0.076 for SF_6–$(Ne)_4$] was more than twice as large as the classical (or $k_{max}=0$) value. In any case, it is clear that if partial averaging is used, even at these relatively low temperatures six Fourier coefficients yield satisfactory convergence for SF_6–$(Ne)_n$ clusters, and two Fourier coefficients for SF_6–$(Ar)_n$ clusters. These conclusions are in accord with those reached by Frantz *et al.*[81] for pure $(Ne)_n$ and $(Ar)_n$ systems.

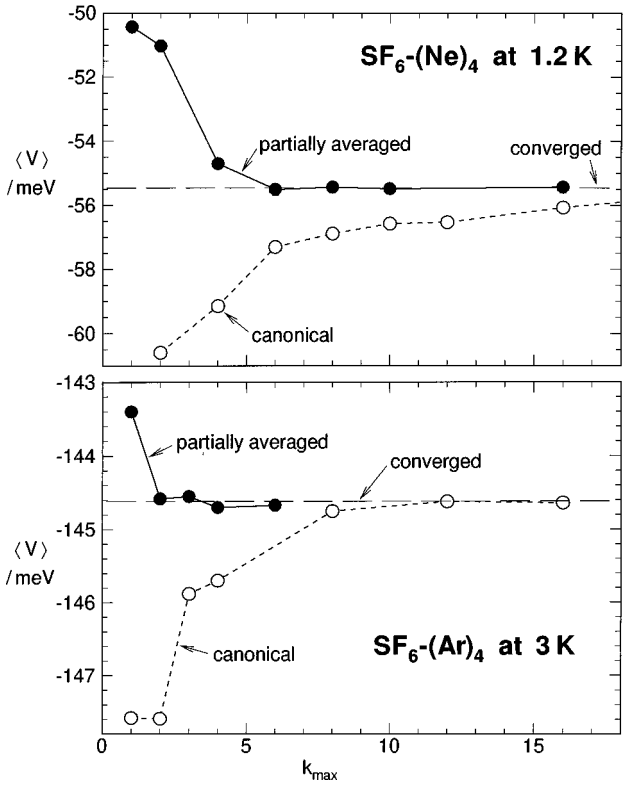

FIG. 2. Illustrative convergence tests for PIMC calculations for SF_6–$(Ar)_4$ and SF_6–$(Ne)_4$, performed with (solid points and curves) and without (open points and dashed curves) using the Coalson *et al.* (Ref. 67) partial averaging procedure.

These and other tests seem to indicate that in general, convergence for simulations using partial averaging is achieved when k_{max} is chosen such that the variance of the distribution of FC moves (σ_{ki}) was $\sim$3.5% of the equilibrium Rg–Rg separation. However, since the largest contributions to the quantum fluctuations come from the lowest-order FC coefficients, biasing the choice of which coefficient to vary to favor them should improve convergence. This was done by selecting the coefficient k to be varied from a Gaussian distribution with variance $k_{max}/2$.

For SF_6–$(Ne)_4$ at 1.2 K, analogous tests of the convergence of calculated properties with respect to the number of Gaussian quadrature points used to evaluate the integrals in Eq. (8) are shown in Fig. 3. These results were generated

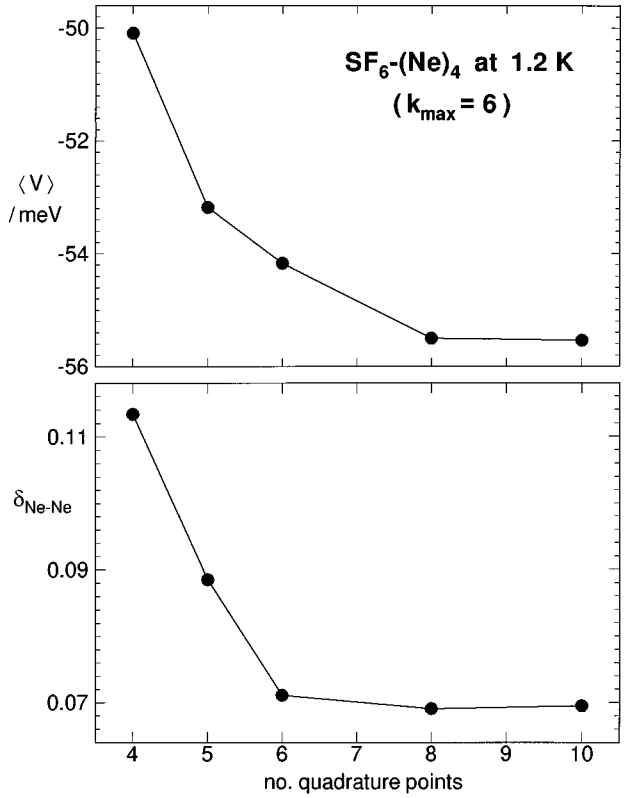

FIG. 3. Illustrative convergence tests for PIMC calculations for SF_6–$(Ne)_4$ at 1.2 K, performed using partial averaging with $k_{max}=6$.

using partial averaging with $k_{max}=6$. For this case it is clear that eight Gaussian quadrature points are needed to yield full convergence; this agrees with what Frantz *et al.*[81] found for pure $(Ne)_n$ clusters. Similar tests for SF_6–$(Ar)_n$ clusters showed that six quadrature points should be used in simulations with $k_{max}=2$. However, for special cases of extremely low temperatures where much larger values of k_{max} are required (see below), the number of quadrature points was set equal to k_{max}.

As a final test of the present procedure, ''melting curves'' of $\delta(T)$ vs T were calculated for the pentagonal pyramid $(Ne)_7$ and icosahedral $(Ne)_{13}$ clusters. Within the accuracy of the plots, the results obtained were identical to those reported by Beck *et al.*[62] and Chakravorty,[63] with the temperature associated onset of melting being, respectively, ~20% and 13% smaller for the PIMC than the classical simulation.[89]

In view of these results, all of the PIMC simulation results presented below were obtained using partial averaging. Except where indicated otherwise, the Ne cluster calculations were performed with $k_{max}=6$ using eight quadrature points, while the Ar cluster results used $k_{max}=2$ with six-quadrature points. Because of its large mass and large rotational moment of inertia, it was assumed that the SF_6 could be treated as a purely classical particle ($k_{max}=0$), so it was held fixed and its centre treated as the coordinate origin for the simulations. Both the PIMC and classical simulations were typically based on $5-10\times10^6$ accepted MC moves (and more for temperatures near melting transitions), with the length

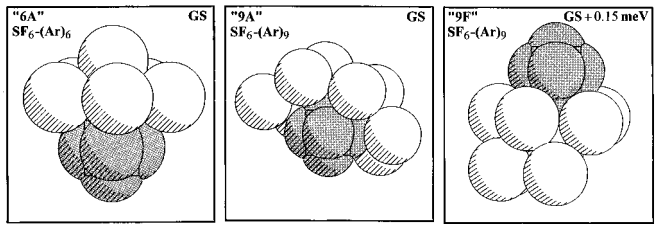

FIG. 4. Structures of selected monolayer and stacked isomers of SF_6–$(Ar)_n$; GS identifies the ground state isomer.

scale for the randomly chosen coordinate displacement being chosen so as to yield an acceptance ratio of approximately 50%.

III. QUANTUM EFFECTS IN SF_6–$(Ar)_n$ CLUSTERS

A. Melting behavior, and relative stability of ''stacked'' vs monolayer isomers

As mentioned above, some of the most interesting results yielded by classical Monte Carlo and molecular dynamics simulations of SF_6–$(Ar)_n$ clusters arose from the special stability of certain competing isomeric forms of those species. While quantum corrections are expected to be relatively modest in systems formed from such heavy atoms,[62] it is still possible that tunneling and zero-point energy effects could reduce or effectively remove barriers between different configurations, and hence cause some of this unusual behavior to disappear. The present section examines this possibility, and compares the magnitude of quantum effects in these systems with the effect on predicted cluster behavior of including three-body forces in the representation of the overall system potential energy function.

Structures of the three isomeric forms of SF_6–$(Ar)_n$ considered here are shown in Fig. 4. They are the ground-state pentagonal-pyramid ''cap'' structure of SF_6–$(Ar)_6$, the ground-state monolayer isomer (structure ''9A'' in Ref. 34) of SF_6–$(Ar)_9$, and a nearly isoenergetic (only 0.15 meV less stable) ''stacked'' structure of SF_6–$(Ar)_9$ (''9F'' in Ref. 34) in which six atoms form a pentagonal pyramid cap on one end of the SF_6 while the three additional atoms sit in a second layer, approximately 7 Å from the center of the SF_6. Details of the potential energy hypersurface make this pentagonal–pyramid cap structure unusually stable, and it is an integral component of the substructure on which many multilayer ''phase-separated'' or ''stacked'' clusters isomers are built.[34,90] The stability of this six-atom cap is also important to the dynamics of these argon clusters, since isomerizations often occur between maximally solvated isomers and stacked structures which have the six-argon-atom cap as a foundation block of their first layer.[30,32,33,56,90] If the relative stability of this structure is decreased significantly, the very existence of stacked structures which have this six-atom cap in the first layer could come into question.

For the three isomers shown in Fig. 4, Fig. 5 presents melting curves (plots of δ_{Ar-Ar} vs T) obtained from four different types of calculations. Results labeled ''CMC'' (open points joined by dashed lines) were obtained from conventional classical Monte Carlo simulations, while those la-

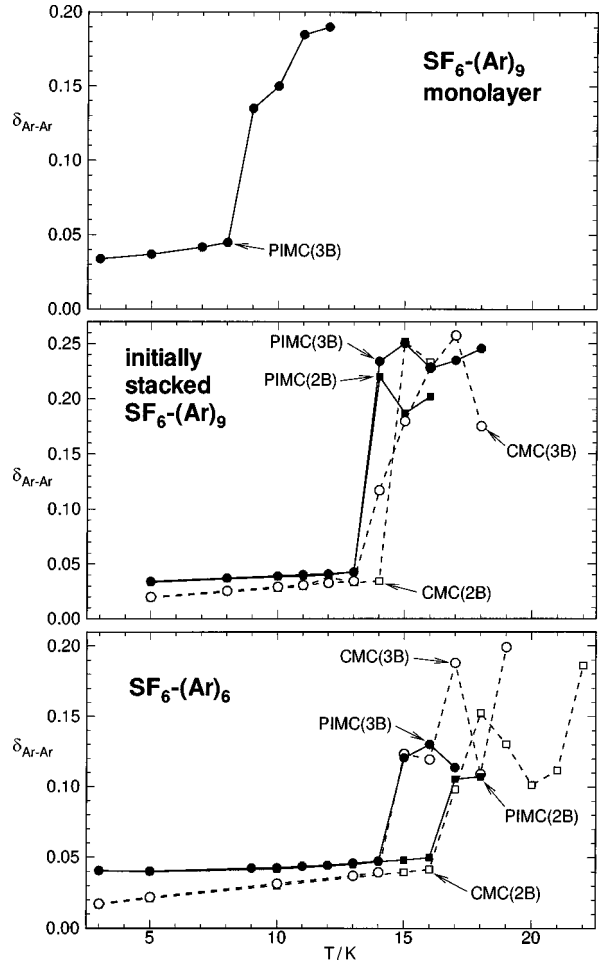

FIG. 5. Melting curve plots for three selected isomers of SF_6–$(Ar)_n$ obtained using classical (open points, dashed curves) and quantum PIMC (solid points, solid curves) simulations which either included (round points, labeled ''3B'') or neglected (square points labeled ''2B'') the three-body ATM interactions.

beled ''PIMC'' (solid points joined by solid lines) were obtained from Fourier path integral quantum Monte Carlo calculations; similarly, results labeled ''2B'' (square points) were obtained using only pairwise-additive potentials, while those labeled ''3B'' (round points) were obtained from simulations which also took account of the three-body ATM interactions. Quantum effects give rise to a twofold increase in the magnitude of the bond length fluctuation parameter $\delta_{\mathrm{Ar–Ar}}$, at the lowest temperatures considered, but have little effect on their qualitative behavior. In contrast, inclusion of the three-body ATM potential terms has little effect on the magnitude of $\delta_{\mathrm{Ar–Ar}}$ for these very low temperature solidlike clusters.

As discussed in Sec. II C, the melting transition is associated with the onset of the sharp rise in $\delta_{\mathrm{Ar–Ar}}(T)$ seen in these plots. The uncertainty in these melting point determinations is mainly due to ''quasiergodicity,'' or incomplete sampling of configuration space, in the simulations. An effort was made to minimize this problem by using the ''jump–walking'' technique[81,91] of periodically increasing the particle coordinate step size and running the simulation with this larger step approximately 20% of the time, in order to facilitate the system accessing relatively distant configurations. In addition, the length of the simulation runs for temperatures near (suspected) melting transitions were often doubled. In any case, the uncertainty in the present melting temperatures of heterogeneous SF_6–$(Ar)_n$ clusters is believed to be approximately ± 0.5 K.

The behavior of the $\delta_{\mathrm{Ar–Ar}}(T)$ plots for SF_6–$(Ar)_6$ is believed to be representative for this family of clusters; its qualitative structure is identical to that found in analogous comparative simulations of the melting of the pentagonal bipyramid isomer of $(Ar)_7$.[92] It shows that quantum effects on the melting temperature of this system are negligible, although including the three-body ATM potential energy terms had the effect of substantially lowering the melting temperature (by ~ 2 K or 13%). Within our (± 0.5 K) uncertainties the same conclusions hold true for the ''stacked'' SF_6–$(Ar)_9$ isomer, although the melting temperature decrease due to the destabilizing three-body terms is somewhat smaller for this less rigid species. Similarly, while classical and ''2B'' Monte Carlo simulations were not run for the SF_6–$(Ar)_9$ monolayer isomer, classical ''2B'' molecular dynamics simulations of this system[93] yielded a melting temperature approximately 1 K higher than that implied by the PIMC (3B) results seen here; in view of the results of Ref. 35, we attribute this difference to our inclusion of the three-body ATM interactions, and not to quantum effects.

In general, the PIMC(3B) melting temperatures of ~ 14.5, 13.5, and 8.5(± 0.5) K must be considered the most accurate values for these species. However, classical Monte Carlo calculations also give essentially equivalent description of this melting behavior. In contrast, as was seen in Ref. 35, addition of the destabilizing ATM terms to the pairwise additive potential energy surface causes distinct reductions in melting temperatures of clusters formed from Ar. The most important present result, however, is the fact that taking account of quantum effects *did not* destabilize the ''stacked'' vs the ''monolayer'' isomers of SF_6–$(Ar)_9$. The integrity of the former means that the size-dependent selective solvation[34] and ''reverse melting'' [30] reported for these systems are *not* artifacts of classical mechanics.

B. Quantum effects on simulated IR spectra

Previous classical (molecular dynamics) simulation studies indicated that the shifts and splittings of the perturbed infrared spectrum of the ν_3 band of SF_6 in a rare gas cluster provide a discriminating means of identifying a particular cluster isomer, and (sometimes) also for determining whether it is behaving like a solid or a liquid.[33] However, quantum effects allow a system to access a relatively wider range of configurations, and hence may be expected to broaden the predicted spectral features. It is therefore appropriate to examine whether such broadening would sufficiently obscure the details of the spectrum that it would no longer provide a sharp diagnostic means of identifying a particular cluster isomer and its dynamical state.

For the ground-state ''9A'' monolayer isomer and the specially stable two-layer (6+3) ''stacked'' isomer ''9F'' of SF_6–$(Ar)_9$, Figs. 6 and 7 compare simulated spectra of the ν_3 band of SF_6 generated from classical (CMC) and quantum

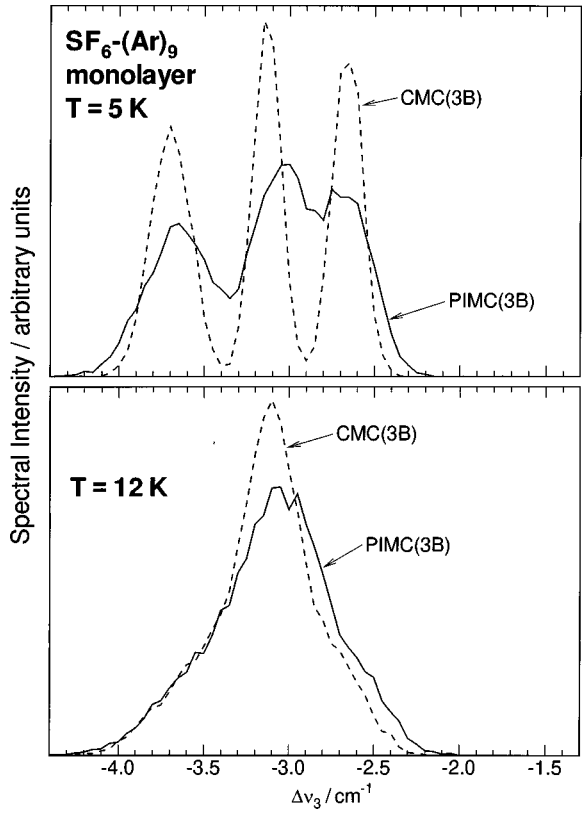

FIG. 6. Predicted shifted spectra of the ν_3 band of SF_6 yielded by classical (dashed curves) and quantum (solid curves) simulations for the monolayer (initially ''9A'') isomer of SF_6–$(Ar)_9$.

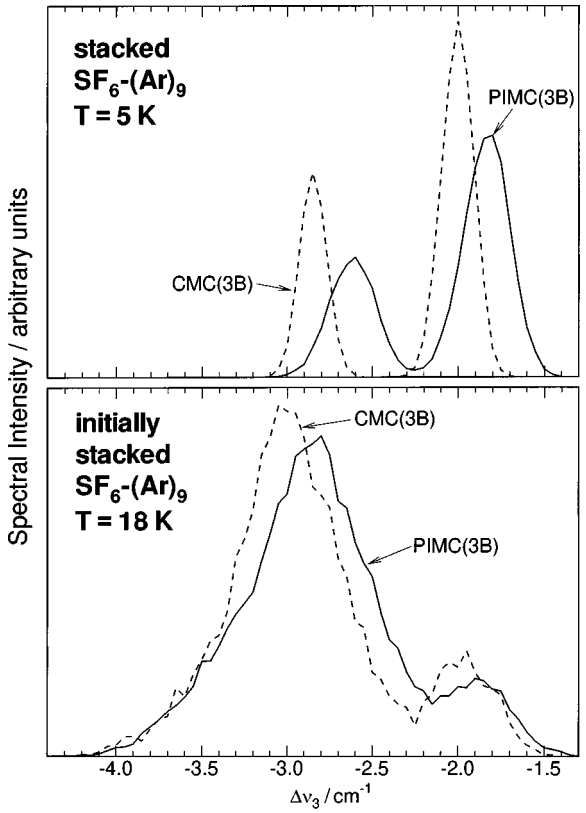

FIG. 7. Predicted shifted spectra of the ν_3 band of SF_6 yielded by classical (dashed curves) and quantum (solid curves) simulations for the initially-stacked $6+3$ isomer ''9F'' of SF_6–$(Ar)_9$.

(PIMC) simulations at temperatures above and below their respective melting transitions, using the full potential energy surface (including the three-body ATM terms). For both species, the PIMC spectra at 5 K clearly retain the distinctive triplet and doublet band splittings previously observed in classical molecular dynamics simulations for these isomers.[33] Although the broader peaks in the PIMC spectra of the monolayer form overlap considerably more than for the classical simulation, the underlying triplet and doublet structures characteristic of the two rigid forms are still clearly resolved. Similarly, at the higher temperatures the collapse of these structures to the single broad peak associated with a maximally solvated liquidlike Ar monolayer is qualitatively the same in both the classical and PIMC calculations. For the (initially) stacked ''9F'' spectrum at 18 K, the small residual CMC and PIMC peaks centered near a shift (from the free monomer transition frequency) of $-2\ \mathrm{cm}^{-1}$ are merely a residual ''memory'' of the perpendicular band component of the doublet spectrum of the rigid two-layer isomer, whose presence indicates that these particular simulations runs were not fully equilibrated before collection of the thermally averaged properties commenced;[94] in a longer simulation, this residual second peak would disappear. Note that the non-Gaussian shape of the limiting high temperature spectra (more easily seen in Fig. 6) illustrates the continuous isomerization between the ''9A'' and ''9B'' monolayer arrangements of the liquidlike system, as discussed in Ref. 33 (see its Fig. 4).

Spectra were also generated from the quantum PIMC(3B) simulations for the monolayer isomer of SF_6–$(Ar)_9$ at all of the other temperatures considered in the uppermost segment of Fig. 5. While the spectra tended to gradually broaden with increasing temperature, at the melting temperature of $8.5(\pm 0.5)$ K they showed an abrupt transition from the low-T triplet to the high-T single-peak structures seen in Fig. 6. Thus, the ability of these spectra to clearly discriminate between the solidlike and liquidlike forms of these species is not affected by the spectral broadening introduced by taking account of quantum effects.

While their general structures are unaffected, the calculated quantum PIMC (3B) spectra seen in Figs. 6 and 7 are all shifted slightly less far to the red of the free monomer line than are the corresponding classical CMC(3B) spectra. This reflects the fact that quantum simulations include contributions from tunneling into classically forbidden regions of configuration space, and the anharmonicity of the SF_6–Ar pair potential means the system spends relatively more time at larger separations for which the contributions to the frequency shifts are relatively small.[29] This conclusion is confirmed by examination of the radial distribution functions associated with these calculations.[89] Similarly, the increase in the average red shift accompanying melting of the stacked SF_6–$(Ar)_9$ cluster (see Fig. 7) simply reflects the fact that on melting, the bilayer stacked structure collapses, so that all atoms make equivalent (relatively large) contributions to the overall shift.

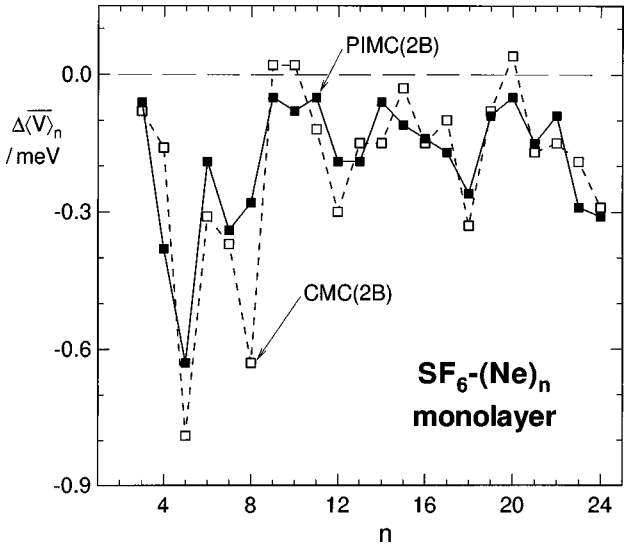

FIG. 8. Changes in the average potential energy per Ne solvent atom in monolayer SF_6–$(Ne)_n$ clusters at 1 K, as additional Ne atoms are added to the system.

IV. QUANTUM EFFECTS IN CLUSTERS FORMED FROM NEON

A. "Pulling, packing, and stacking": Structural proclivities of SF_6–$(Ne)_n$ clusters

As pointed out in Ref. 34, the potential energy curves governing SF_6–$(Rg)_n$ clusters for Rg=Ne (and He) are qualitatively distinctly different than those for the heavier rare gas atoms. In particular (see Fig. 1), the Ne–Ne binding energy is much weaker relative to both the overall strength and the anisotropy of the Ne–SF_6 interaction, than is the case for the heavier Rg partners, and its equilibrium distance is distinctly smaller relative to that for the Ne–SF_6 potential. Thus, it is reasonable to expect that its proclivities for forming different types of structures will be markedly different. In particular, the relative weakness of the Ne–Ne potential should more strongly favor maximally-solvated rather than phase-separated structures, since there will be less advantage gained on forming close packed structures by ejecting the SF_6 to the surface of the cluster. Moreover, the special stability of the underlayer of stacked SF_6–$(Ar)_n$ species is at least partly due to the strength of the anisotropy of the Ar–SF_6 interaction,[34,90] so this relatively weaker anisotropy will also tend to destabilize phase-separated forms of SF_6–$(Ne)_n$.

The sort of detailed cataloging and analysis of the nature and relative energies of different cluster isomers reported[34] for SF_6–$(Ar)_n$ and SF_6–$(Kr)_n$ was not undertaken here. However, some effort was made to survey the patterns of cluster energies in order to understand whether or not certain types of structures would be particularly stable. This question is relevant because the rigidity of particular first-layer-atom structures is a key feature determining the stability of associated multilayer structures. To this end, simulated annealing was used to determine the average potential energies of very low temperature equilibrated monolayer SF_6–$(Ne)_n$ clusters. The results of this survey are summarized in Fig. 8, which shows how the 1 K thermal average of the potential energy per Ne atom in an SF_6–$(Ne)_n$ cluster changes as additional atoms are added to the system,

$$\Delta\overline{\langle V\rangle}_n = \langle V(SF_6\text{–}Ne_n)\rangle/n - \langle V(SF_6\text{–}Ne_{n-1})\rangle/(n-1). \tag{9}$$

In view of the relatively small magnitudes of the three-body ATM coefficients involving Ne (see Table I), many-body interactions are not expected to be very important for these systems (see also below), so these calculations used only the pairwise-additive two-body potentials. Since the PIMC method is inherently a finite temperature approach, the quantum averaging had to be done at a finite temperature (1 K), and for the sake of consistency the classical results shown were obtained in the same way. However, converging the latter to 0 K (the absolute potential minima) merely reduces each value of $\langle V(SF_6\text{–}Ne_n)\rangle/n$ by $1.5k_BT$, so the classical differences (open "CMC" points in Fig. 8) are essentially identical to the changes in the associated absolute potential minima. For this family of systems, the first Ne atom shell around the SF_6 becomes full at $n=24$, which compares to $n=20$ for Ar and $n=17$ for Kr,[34] and to $n=23$ for He.[36,37]

The classical results (open points joined by dashed lines) in Fig. 8 suggest that particular stable monolayer structures occur for $n=5$ and 8. The first of these corresponds to a tetragonal pyramid arrangement in which one Ne atom lies on one of the S–F bond axes and the other four are approximately centered in neighboring pockets near three fold Ne–SF_6 symmetry axes; the second consists of two asymmetric tetragonal pyramids sharing two base atoms. The strong preference for these structures reflects the fact that the Rg–Rg interaction is much weaker relative to the Rg–SF_6 potential anisotropy than is the case for the analogous Ar and Kr systems where a pentagonal pyramid structure centered on one of the S–F axes is more important.

The quantum results (solid points and lines) show that zero-point energy effects generally reduce the differences among the relative stabilities of the different structures, and in the case of SF_6–$(Ne)_8$ largely removes the special stability associated with that particular arrangement. The effect of quantum corrections in reducing the stability of these monolayer Ne structures has implications regarding the existence of phase-separated forms of these species.

Independent molecular dynamics simulated annealing calculations showed that a wide variety of stacked or phase-separated isomers could classically exist for these species.[95] However, in all cases they were metastable relative to monolayer structures; this differs from the situation for SF_6–$(Ar)_n$ and SF_6–$(Kr)_n$, where the phase-separated or stacked structures are the lowest energy forms for many cluster sizes.[34] It

TABLE I. Triple–dipole dispersion energy coefficients for the species of interest, in units [hartree×(bohr)^9]; their estimated uncertainties are $\lesssim 2\%$.[a]

	Rg=Ne	Ar	Kr
SF_6–$(Rg)_2$	118.43	1467.19	3047.70
$(Rg)_3$	11.95	518.34	1571.55

[a]References 35, 65, 66.

is also interesting to note that in spite of the special classical *and* quantum stability of the $n=5$ structure (see Fig. 8), no classically stable two-layer structures could be built on it, as the relatively large Ne–Ne separations too easily allowed any additional atoms to drop down into a monolayer.

B. Quantum vs three-body interaction effects on SF_6–$(Ne)_n$ cluster melting

As shown by Eq. (7), the variance of the distribution of Fourier coefficients associated with particles which are treated quantum mechanically is inversely proportional to the square root of the product of the particle mass times the effective temperature. At at given temperature, Ne atoms will therefore show considerably larger quantum effects than Ar atoms. Moreover, since the Ne–Ne well depth (3.64 meV) is less than one-third as large as that for Ar–Ar (12.34 meV), and the average Ne–SF_6 well depth less than half that for Ar–SF_6 (see Fig. 1), SF_6–$(Ne)_n$ clusters will melt at much lower temperatures than SF_6–$(Ar)_n$ clusters. Both of these factors tend to make quantum effects on melting behavior much larger in clusters formed from Ne than in those formed from Ar. At the same time, the relative weakness of the ATM three-body coefficients for Ne (see Table I) suggests that many-body forces will be relatively much less important here than for clusters formed from Ar.

The above hypotheses are confirmed by consideration of melting curve plots of $\delta_{\mathrm{Ne-Ne}}$ vs T for various pure $(Ne)_n$ and SF_6–$(Ne)_n$ clusters. For $(Ne)_7$ and $(Ne)_{13}$ we found that quantum effects lowered the melting temperatures from 3.9 to 3.1 K and from 7.7 to 6.7 K, respectively, in excellent accord with the results Beck *et al.*[62] and Chakravorty[63] obtained using pairwise-additive Lennard-Jones(12,6) interaction potentials, while within our uncertainties (± 0.1 and ± 0.3 K, respectively), inclusion of three-body interactions had no effect on those transition temperatures. Figure 9 presents similar results for SF_6–$(Ne)_6$ and SF_6–$(Ne)_8$, which show that quantum effects substantially lower the melting temperatures, while the destabilizing effect of including the three-body interaction terms is much smaller. Our recommended values for the SF_6–$(Ne)_6$ and SF_6–$(Ne)_8$ melting temperatures are the PIMC values of 2.5 and 2.3(± 0.1) K, respectively.

C. The stability of stacked SF_6–$(Ne)_n$ clusters

As was pointed out above, the relatively much weaker Rg–Rg interaction in SF_6–$(Ne)_n$ clusters leads one to expect that their stacked or phase-separated structures will be much less stable than analogous multilayer SF_6–$(Ar)_n$ and SF_6–$(Kr)_n$ isomers. Classical simulations based on additive two-body interactions confirmed this prediction, but showed that some metastable stacked structures were still classically stable. A question which remains is whether some ''stacked'' or phase-separated SF_6–$(Ne)_n$ structures remain stable when zero-point energies are taken into account, or whether their existence is an artifact of classical mechanics.

We examine this question by first considering the properties of the stacked isomeric structure which is the analog of the most stable phase-separated form found for SF_6–$(Ar)_n$ and SF_6–$(Kr)_n$. This is the SF_6–$(Rg)_{12}$ species ''12F,'' which is the ground state isomer of that size for both Rg=Ar and Kr;[34] it is an icosahedron of Rg atoms with one of the surface atoms replaced by one of the F atoms protruding from the SF_6. The optimal icosahedral Rg–Rg packing of this species gives it special stability, and as with the analogous perfectly icosahedral $(Rg)_{13}$ species,[7,8,71] it has a distinctly higher melting temperature than other ''less-perfect'' structures.[93]

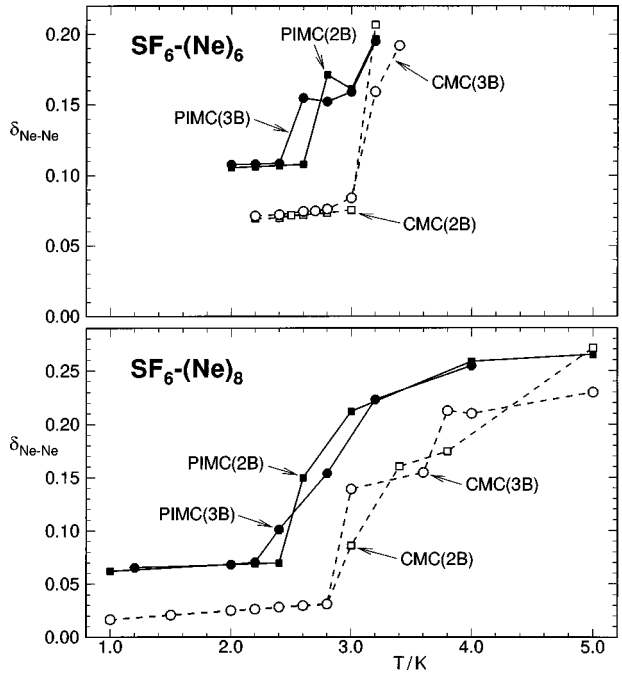

FIG. 9. Melting curve plots for two monolayer isomers of SF_6–$(Ne)_n$ obtained using classical (open points, dashed curves) and quantum PIMC (solid points, solid curves) simulations which either included (round points, labeled ''3B'') or neglected (square points, labeled ''2B'') the three-body ATM interactions.

Melting curves obtained for this species are shown in Fig. 10; the round points correspond to classical (open points and dashed lines) and quantum (solid points and lines) simulations which started from the classical minimum-energy icosahedronlike stacked structure ''12F,'' while the triangular points were obtained from simulations which started from maximally-solvated monolayer structures. At sufficiently low temperatures, $\delta_{\mathrm{Ne-Ne}}$, values for the ''initially-stacked'' species showed the relatively low values and weak temperature dependence associated with solidlike behavior, and radial distribution functions associated with these simulations confirmed that they retained the near-rigid stacked structure throughout the simulation run. However, above their melting transitions [the onset of the abrupt rise in $\delta_{\mathrm{Ne-Ne}}$ at 2.5 (± 0.1) and 3.1(± 0.1) K for the quantum and classical results, respectively], these species abruptly collapsed to a liquidlike monolayer. In contrast, the ''initially-monolayer'' classical results (open triangle points) never really show the nearly-flat temperature dependence normally associated with solidlike behavior, and this is only weakly suggested in the associated quantum results for $T<1.5$ K. Thus, the monolayer form seems to be a plastic phase with no sharp melting

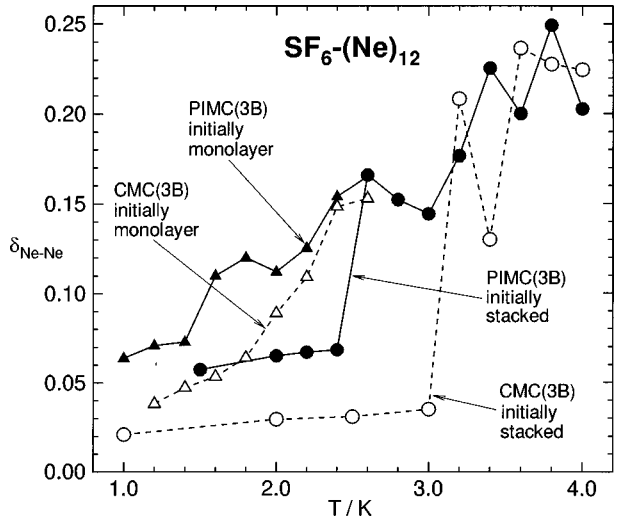

FIG. 10. Classical (open points joined by dashed curves) and quantum (solid points and curves) melting curve plots for two isomeric forms of SF_6–$(Ne)_{12}$. The round points correspond to simulations which always started from the classically-stable icosahedronlike stacked structure, while triangular points were obtained from simulations which started from a monolayer structure.

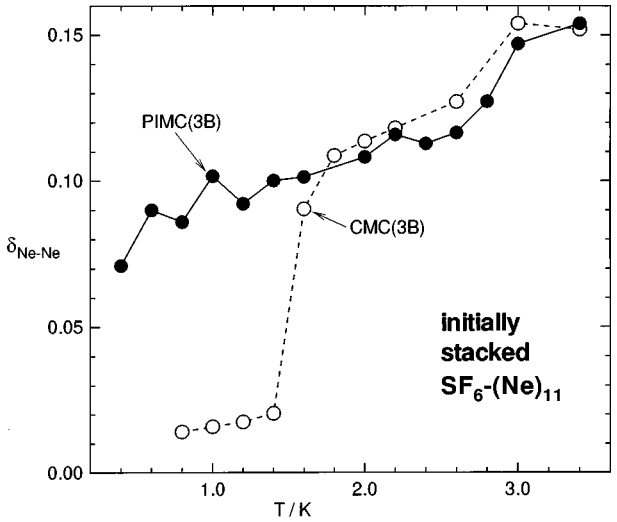

FIG. 11. Classical (open points joined by dashed curves) and quantum (solid points and curves) melting curve plots for the initially-stacked $8+3$ isomer of SF_6–$(Ne)_{11}$.

transition. In view of the relative strengths of the Ne–Ne and Ne–SF_6 potentials (see Fig. 1) this behavior should not be surprising, and it may be expected to occur for many of the larger monolayer species.

The above results show that the stacked SF_6–$(Ne)_{12}$ ''12F'' isomer structure still does exist when quantum effects are taken into account, though as with the smaller monolayer isomers considered in Fig. 9, its melting temperature is sharply lowered. This was also the case for the Ne analog of the other specially-stable stacked structure identified in Ref. 34, isomer ''18E'' of SF_6–$(Ar)_{18}$ and SF_6–$(Kr)_{18}$, in which a ten-atom second layer is stacked on an ''8A''-type[34] first layer. For the analogous SF_6–$(Ne)_{18}$ species, quantum effects reduce the classical melting temperature of $5.25(\pm 0.25)$ K by almost a factor of 2 to 2.9 (± 0.1) K, but the stacked structure still did exist at sufficiently small T. On the other hand, if this much quantum destabilization occurs for these two (classically) specially-stable stacked isomers, the persistence of more ''ordinary'' phase-separated forms of various cluster sizes seems unlikely.

The above prediction seems to be born out by our results for a classically-stable $8+3$ bilayer isomer of SF_6–$(Ne)_{11}$.[96] The eight-atoms in the first layer have the same ''8A''-type arrangement (two tetragonal pyramids sharing one stretched base pair) which the classical results in Fig. 8 showed to be specially stable, so this should be a promising candidate for a stable stacked structure. Classical and quantal $\delta_{\mathrm{Ne-Ne}}(T)$ values for this species are presented in Fig. 11; all simulations started from the classically stable equilibrium stacked structure. The classical results (open points joined by dashed lines) indicate that a solidlike stacked structure persists for $T \leqslant 1.5(\pm 0.1)$ K, above which it collapses to a liquidlike monolayer, but the $\delta_{\mathrm{Ne-Ne}}$ values yielded by the quantum simulation show no evidence of solidlike behavior down to the lowest temperatures considered. Moreover, although all runs started from the classically-stable stacked structure, except for the two very lowest temperatures, all of the quantum runs immediately collapsed to a liquidlike monolayer.[97] At those two very lowest temperatures, 0.6 and 0.4 K, $\delta_{\mathrm{Ne-Ne}}$ retained the relatively large values associated with liquidlike behavior,[98] but a two-layer structure was maintained throughout the course of the simulation.[97] However, since *all* stacked SF_6–$(Ne)_n$ structures are metastable relative to monolayer forms, this is believed to be an artifact of our (very time consuming[98]) simulation being far to short to properly sample the full accessible configuration space. In summary, therefore, we conclude that with the exception of a limited number of ''pathologically-stable'' stacked structures [such as the icosahedral-like isomer of SF_6–$(Ne)_{12}$] which may still exist at extremely low temperatures, when quantum effects are taken into account, phase-separated forms of SF_6–$(Ne)_n$ generally do not exist.

D. IR spectra diagnostics for SF_6–$(Ne)_n$ clusters

In spite of the spectral broadening and a net displacement to smaller (less red) frequency shifts associated with quantum averaging, the simulated IR spectra of SF_6–$(Ne)_n$ clusters still retain the ability to discriminate between different isomeric forms of these species. This is illustrated by Fig. 12, which plots simulated spectra generated for the initially-stacked isomers of SF_6–$(Ne)_{12}$ and SF_6–$(Ne)_{18}$ considered above. In both cases, the splitting into component peaks and small overall shift seen at the lower temperatures is replaced at the higher temperature by the type of single broad peak and larger overall shift associated with heterogeneous averaging over the variety of monolayer structures associated with liquidlike behavior. The asymmetry of this high temperature spectrum for SF_6–$(Ne)_{18}$ reflects the fact that normal fluctuations allow the system to spend part of its time in multilayer forms which have smaller average frequency shifts.

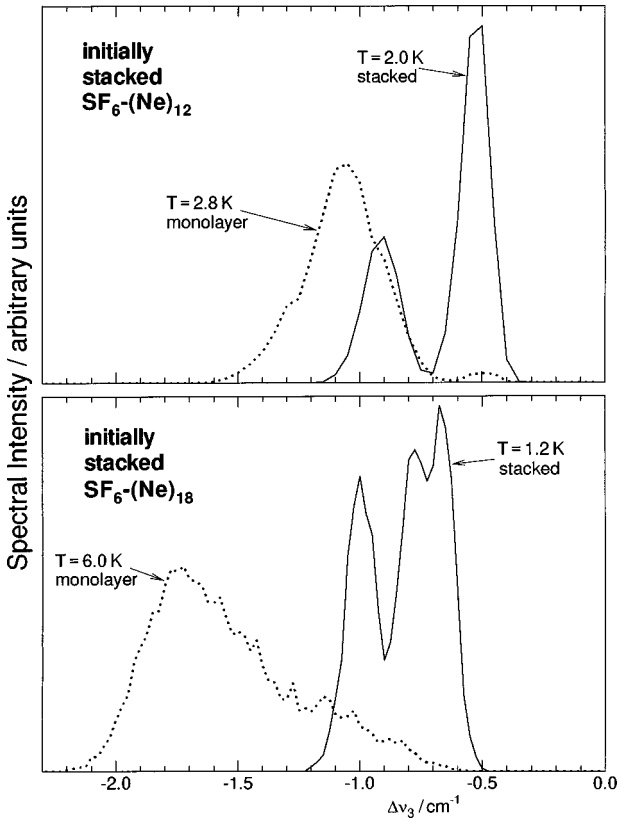

FIG. 12. Predicted shifted spectra of the ν_3 band of SF_6 yielded by quantum PIMC simulations of initially-stacked isomers of SF_6–$(Ne)_{12}$ and SF_6–$(Ne)_{18}$. In both cases, at the higher temperature the system collapses to the monolayer form during the simulation run.

V. DISCUSSION AND CONCLUSIONS

Most previous simulations of ''heavy'' (i.e., not involving He or H_2) heterogeneous clusters have been based on the use of classical Monte Carlo or molecular dynamics calculations, and the present work was undertaken to examine whether quantum effects would affect the physical conclusions drawn from that work. One property of particular interest is the selective size-dependence of the proclivity for maximal solvation vs phase separation found for the SF_6–$(Ar)_n$ and SF_6–$(Kr)_n$ systems.[34] Another is the phenomenon of ''reverse melting,'' where heating a liquidlike monolayer or maximally-solvated species allows it to isomerize into a long-lived solidlike phase-separated form.[30,31,93] Both of these phenomena, as well as the magnitude of the quantum effects themselves, depend on the particle masses, the temperature, and the relative strengths and anisotropies of the like- and unlike-pair interaction potentials. A matter of further interest, was ascertaining the implications for more weakly bound mixed clusters formed from Ne.

To address these questions, the results of classical Monte Carlo and Fourier path integral quantum Monte Carlo calculations have been compared for a range of SF_6–$(Rg)_n$ clusters of different sizes and types. For SF_6–$(Ar)_n$ systems, quantum corrections were found to have little effect on the melting temperatures, simulated spectra, or relative stability of phase-separated vs maximally-solvated isomers. In particular, the lack of effect on the melting temperature of even the stacked ''9F'' isomer of SF_6–$(Ar)_9$ affirms that for clusters formed from Ar, and by extension also those formed from heavier solvent partners, the size-dependent selective solvation and reverse melting observed for such species are not artifacts of classical mechanics. Moreover, in spite of shifts and broadening due to quantum tunneling and zero point energy averaging, the simulated spectra retain the ability to clearly discriminate between different cluster sizes and isomeric structures, and between solidlike and liquidlike forms of these species. At the same time, present results reaffirm the conclusion of Ref. 35 that inclusion of the three-body ATM triple–dipole interaction energy leads to significant reductions in the melting temperatures of both stacked and solvated forms of SF_6–$(Ar)_n$, and presumably also those of other heavy-solvent systems.

For the analogous SF_6–$(Ne)_n$ systems, the situation was found to be quite different. Here effects of three-body interaction terms are almost negligible, and the relative weakness of the Rg–Rg vs the Rg–SF_6 pair interaction makes even the classical stability of stacked or phase-separated isomeric forms more precarious. In particular, unlike the Ar and Kr systems, maximally solvated SF_6–$(Ne)_n$ isomers were found classically to be the ground state forms for *all* cluster sizes examined, although classically stable phase-separated isomers of SF_6–$(Ne)_n$ do exist for a range of cluster sizes. However, quantum effects on their melting temperatures are quite large, lowering those for the monolayer isomers studied by $\sim$20%. Quantum effects on the stability of phase-separated or stacked forms were even more drastic. For the ''18E'' SF_6–$(Ne)_{18}$ and the icosahedral-like ''12F'' SF_6–$(Ne)_{12}$ bilayer isomers, which the studies of SF_6–$(Ar)_n$ and SF_6–$(Kr)_n$ suggest should be specially stable,[34] quantum effects lowered the melting temperatures by 45% and 20%, respectively. Moreover, our results for a more ''ordinary'' representative $8+3$ stacked isomer of SF_6–$(Ne)_{11}$ showed that while it *classically* retained a solidlike stacked structure for for temperatures below $1.5(\pm 0.5)$ K, the quantum results showed no evidence of solidlike behavior down to the lowest temperatures considered,[98] and we conclude that initially-stacked forms of this species will always collapse to a liquidlike maximally-solvated form. We therefore conclude that with the exception of a limited number of ''pathologically-stable'' stacked isomers [such as the icosahedral-like form of SF_6–$(Ne)_{12}$] which can still exist at extremely low temperatures, when quantum effects are taken into account, phase-separated forms of SF_6–$(Ne)_n$ generally do not exist.

The present work also completes the determination of the preferred positions of an SF_6 dopant molecule in rare gas clusters. The detailed structural simulation study of Ref. 34 concluded that although the preference for maximal solvation vs phase separation in SF_6–$(Ar)_n$ and SF_6–$(Kr)_n$ varied with cluster size up to closure of the first solvent shell, for larger clusters the Kr species would perferentially be phase separated while the analogous Ar clusters would preferentially be maximally solvated. Arguments based on the relative strengths of the Rg–Rg vs Rg–SF_6 interaction potentials suggested that clusters formed from Ne and He would also preferentially be solvated, while the SF_6 would preferentially lie at the surface of clusters formed with Xe.[34] Experiment

has since confirmed these predictions for Rg=Ar, Kr, and Xe,[25] and both theory and experiment agree that SF_6 is fully solvated in large He clusters.[24,36,37,99] The present results complete this series by showing that while particular stacked SF_6–$(Ne)_n$ isomers can exist, they are metastable, and in general SF_6 will also be maximally solvated in Ne clusters. It is reassuring to see that this trend in behavior can be readily explained by consideration of the relative strengths of the forces between the like and unlike particles forming the cluster,[34] a result which attests to the prescience of the numerical study of dopant solvation by Perera and Amar.[14]

Finally, we note that although quantum effects broaden and decrease the overall (red) IR frequency shifts of the SF_6 ν_3 band, the simulated (and hence experimental!) spectra still retain the ability to distinguish between different isomeric forms of SF_6–$(Ne)_n$ clusters.

ACKNOWLEDGMENTS

We are pleased to acknowledge helpful discussions with Professor T. Beck which greatly facilitated our learning to understand and use the PIMC method, and we are pleased to thank Professors A. Kumar and W. J. Meath for providing their unpublished triple–dipole dispersion energy coefficient for SF_6–$(Ne)_2$. Funding for this research was provided by the Natural Sciences and Engineering Research Council of Canada through the Network of Centres of Excellence in Molecular and Interfacial Dynamics.

[1] M. Kappes and S. Leutwyler, in *Atomic and Molecular Beam Methods*, edited by G. Scoles, D. Bassi, U. Buck, and D. Laine (Oxford University Press, Oxford, 1988), Vol. 1, Chap. 15.
[2] U. Hefter and K. Bergmann, in *Atomic and Molecular Beam Methods*, edited by G. Scoles, D. Bassi, U. Buck, and D. Lainé (Oxford University Press, Oxford, 1988), Vol. 1, Chap. 9.
[3] T. Gough, in *Atomic and Molecular Beam Methods*, edited by G. Scoles, D. Lainé, and U. Valbusa (Oxford University Press, Oxford, 1992), Vol. 2, Chap. 1.
[4] R. E. Miller, in *Atomic and Molecular Beam Methods*, edited by G. Scoles, D. Lainé, and U. Valbusa (Oxford University Press, Oxford, 1992), Vol. 2, Chap. 6.
[5] S. Goyal, D. L. Schutt, and G. Scoles, Acc. Chem. Res. **26**, 123 (1993).
[6] J. K. Lee, J. A. Barker, and F. F. Abraham, J. Chem. Phys. **68**, 1325 (1978).
[7] J. B. Kaelberer and R. D. Etters, J. Chem. Phys. **66**, 3233 (1977).
[8] R. D. Etters and J. B. Kaelberer, J. Chem. Phys. **66**, 5112 (1977).
[9] C. L. Briant and J. J. Burton, J. Chem. Phys. **63**, 2045 (1975).
[10] R. S. Berry, in *The Chemical Physics of Atomic and Molecular Clusters*, in *Proceeding of Course CVII of the International School of Physics ''Enrico Fermi,''* edited by G. Scoles (North–Holland, Amsterdam, 1990), Chaps. 1 and 2.
[11] R. S. Berry, in *Large Finite Systems*, in *Proceedings of the 20th Jerusalem Symposium on Quantum Chemistry and Biochemistry*, edited by J. Jortner and B. Pullman (Reidel, Dordrecht, 1987), pp. 135–143.
[12] T. L. Beck and R. S. Berry, J. Chem. Phys. **88**, 3910 (1987).
[13] I. L. Garzon, X. P. Long, R. Kawai, and J. H. Weare, Chem. Phys. Lett. **158**, 525 (1989).
[14] L. Perera and F. G. Amar, J. Chem. Phys. **93**, 4884 (1990).
[15] T. E. Gough, R. E. Miller, and G. Scoles, J. Chem. Phys. **69**, 1588 (1978).
[16] T. E. Gough, R. E. Miller, and G. Scoles, J. Phys. Chem. **85**, 4041 (1981).
[17] T. E. Gough, D. G. Knight, and G. Scoles, Chem. Phys. Lett. **97**, 155 (1983).
[18] T. E. Gough, M. Mengel, and P. A. Rowntree, J. Chem. Phys. **83**, 4958 (1986).
[19] D. J. Levandier, S. Goyal, J. McCombie, B. Pate, and G. Scoles, J. Chem. Soc., Faraday Trans. **86**, 2361 (1990).
[20] X. J. Gu, D. J. Levandier, B. Zhang, G. Scoles, and D. Zhuang, J. Chem. Phys. **93**, 4898 (1990).
[21] S. Goyal, G. N. Robinson, G. L. Schutt, and G. Scoles, J. Phys. Chem. **95**, 4186 (1991).
[22] S. Goyal, D. L. Schutt, and G. Scoles, Phys. Rev. Lett. **69**, 933 (1992).
[23] S. Goyal, D. L. Schutt, and G. Scoles, Chem. Phys. Lett. **196**, 123 (1992).
[24] R. Fröchtenicht, J. P. Toennies, and A. Vilesov, Chem. Phys. Lett. **229**, 1 (1994).
[25] S. Goyal, D. L. Schutt, and G. Scoles, J. Chem. Phys. **102**, 2302 (1995).
[26] M. Hartmann, R. E. Miller, J. P. Toennies, and A. Vilesov, Phys. Rev. Lett. **75**, 1566 (1995).
[27] D. Eichenauer and R. J. Le Roy, Phys. Rev. Lett. **57**, 2920 (1986).
[28] R. J. Le Roy, J. C. Shelley, and D. Eichenauer, in *Large Finite Systems*, in *Proceedings of the 20th Jerusalem Symposium on Quantum Chemistry and Biochemistry*, edited by J. Jortner and B. Pullman (Reidel, Dordrecht, 1987), pp. 165–172.
[29] D. Eichenauer and R. J. Le Roy, J. Chem. Phys. **88**, 2898 (1988).
[30] J. C. Shelley, R. J. Le Roy, and F. G. Amar, Chem. Phys. Lett. **152**, 14 (1988).
[31] R. J. Le Roy, in *The Chemical Physics of Atomic and Molecular Clusters*, in *Proceedings of Course CVII of the International School of Physics ''Enrico Fermi,''* edited by G. Scoles (North–Holland, Amsterdam, 1990), pp. 137–158.
[32] R. J. Le Roy, J. C. Shelley, D. J. Chartrand, and M. A. Kmetic, in *The Dynamics of Polyatomic van der Waals Complexes*, edited by N. Halberstadt and K. C. Janda (Plenum, New York, 1990), p. 371.
[33] M. A. Kmetic and R. J. Le Roy, J. Chem. Phys. **95**, 6271 (1991).
[34] D. J. Chartrand, J. C. Shelley, and R. J. Le Roy, J. Phys. Chem. **95**, 8310 (1991).
[35] D. J. Chartrand, R. J. Le Roy, A. Kumar, and W. J. Meath, J. Chem. Phys. **98**, 5668 (1993).
[36] R. N. Barnett and K. B. Whaley, J. Chem. Phys. **99**, 9730 (1993).
[37] Y. Kwon, D. M. Ceperley, and K. B. Whaley, J. Chem. Phys. **104**, 2342 (1996).
[38] M. A. McMahon, R. N. Barnett, and K. B. Whaley, J. Chem. Phys. **104**, 5080 (1996).
[39] R. A. Aziz and M. J. Slaman, Chem. Phys. **130**, 187 (1989).
[40] R. A. Aziz and M. J. Slaman, Mol. Phys. **58**, 679 (1986).
[41] R. A. Aziz and M. J. Slaman, Chem. Eng. Commun. **78**, 153 (1989).
[42] R. T Pack, E. Piper, G. A. Pfeffer, and J. P. Toennies, J. Chem. Phys. **80**, 4940 (1984).
[43] R. T Pack, J. J. Valentini, and J. B. Cross, J. Chem. Phys. **77**, 5486 (1982).
[44] B. M. Axilrod and E. Teller, J. Chem. Phys. **11**, 299 (1943).
[45] Y. Muto, Proc. Phys. Soc. Jpn. **17**, 629 (1953).
[46] J. A. Barker, in *Rare Gas Solids*, edited by M. L. Klein and J. A. Venables (Academic, New York, 1976), Chap. 4.
[47] J. A. Barker, J. Chem. Phys. **86**, 1509 (1987).
[48] J. A. Barker, J. Stat. Phys. **52**, 1359 (1988).
[49] J. A. Barker and A. Pompe, Aust. J. Chem. **21**, 1683 (1968).
[50] J. K. Lee, J. A. Barker, and G. M. Pound, J. Chem. Phys. **60**, 1976 (1974).
[51] J. Miyazaki, J. A. Barker, and G. M. Pound, J. Chem. Phys. **64**, 3364 (1976).
[52] W. J. Meath and R. A. Aziz, Mol. Phys. **52**, 225 (1984).
[53] W. J. Meath and M. Koulis, J. Mol. Struct.: THEOCHEM **226**, 1 (1991).
[54] A. D. McLean, B. Liu, and J. A. Barker, J. Chem. Phys. **89**, 6339 (1988).
[55] C. H. J. Johnson and E. H. Spurling, Aust. J. Chem. **24**, 2205 (1971).
[56] J. C. Shelley, M.Sc. thesis, University of Waterloo, 1987.
[57] J. Jellinek, T. L. Beck, and R. S. Berry, J. Chem. Phys. **84**, 2783 (1986).
[58] F. G. Amar and R. S. Berry, J. Chem. Phys. **85**, 5943 (1986).
[59] D. Scharf, G. J. Martyna, and M. L. Klein, J. Chem. Phys. **99**, 8997 (1993).
[60] D. Scharf, G. J. Martyna, D. Li, G. A. Voth, and M. L. Klein, J. Chem. Phys. **99**, 9013 (1993).
[61] R. N. Barnett and K. B. Whaley, Z. Phys. D **31**, 75 (1994).
[62] T. L. Beck, J. D. Doll, and D. L. Freeman, J. Chem. Phys. **90**, 5651 (1989).
[63] C. Chakravarty, J. Chem. Phys. **102**, 956 (1995).
[64] D. L. Freeman and J. D. Doll, J. Chem. Phys. **82**, 462 (1985).
[65] A. Kumar and W. J. Meath, Mol. Phys. **54**, 823 (1985).
[66] A. Kumar and W. J. Meath (private communication, 1991).
[67] M. R. Davies, M.Sc. thesis, University of Waterloo, 1991.
[68] L. H. Jones and B. I. Swanson, J. Chem. Phys. **79**, 1516 (1983).
[69] F. A. Lindemann, Phys. Z. **11**, 609 (1910).

[70] J. J. Gilvarry, Phys. Rev. **103**, 1700 (1956).
[71] T. L. Beck, J. Jellinek, and R. S. Berry, J. Chem. Phys. **87**, 545 (1987).
[72] H. L. Davis, J. Jellinek, and R. S. Berry, J. Chem. Phys. **86**, 6456 (1987).
[73] D. L. Freeman and J. D. Doll, in *Advances in Chemical Physics*, edited by I. Prigogine and S. A. Rice (Wiley, New York, 1988), Vol. 70B, p. 139.
[74] J. D. Doll, D. L. Freeman, and T. L. Beck, in *Advances in Chemical Physics*, edited by I. Prigogine and S. A. Rice (Wiley, New York, 1990), Vol. 78, p. 61.
[75] J. D. Doll, R. D. Coalson, and D. L. Freeman, Phys. Rev. Lett. **55**, 1 (1985).
[76] D. Thirumalai, R. W. Hall, and B. J. Berne, J. Chem. Phys. **81**, 2523 (1984).
[77] R. Q. Topper, G. J. Tawa, and D. G. Trular, J. Chem. Phys. **97**, 3668 (1992).
[78] R. Q. Topper and D. G. Trular, J. Chem. Phys. **97**, 3647 (1992).
[79] D. L. Freeman and J. D. Doll, J. Chem. Phys. **80**, 5709 (1984).
[80] R. D. Coalson, D. L. Freeman, and J. D. Doll, J. Chem. Phys. **85**, 4567 (1986).
[81] D. D. Frantz, D. L. Freeman, and J. D. Doll, J. Chem. Phys. **97**, 5713 (1992).
[82] R. D. Coalson, J. Chem. Phys. **85**, 926 (1986).
[83] R. P. Feynman and A. R. Hibbs, *Quantum Mechanics and Path Integrals* (McGraw–Hill, New York, 1965).
[84] B. J. Berne and D. Thirumalai, Annu. Rev. Phys. Chem. **37**, 401 (1986).
[85] J. D. Doll and L. E. Myers, J. Chem. Phys. **71**, 2880 (1979).
[86] S. W. Rick, D. L. Leitner, J. D. Doll, D. L. Freeman, and D. D. Frantz, J. Chem. Phys. **95**, 6658 (1991).
[87] N. Metropolis, A. W. Rosenbluth, M. N. Rosenbluth, A. H. Teller, and E. Teller, J. Chem. Phys. **21**, 1087 (1953).
[88] M. P. Allen and D. J. Tildesley, *Computer Simulation of Liquids* (Oxford University, Oxford, 1987).
[89] D. J. Chartrand, Ph.D. thesis, University of Waterloo, 1994.
[90] D. J. Chartrand, M.Sc. thesis, University of Waterloo, 1990.
[91] D. D. Frantz, D. L. Freeman, and J. D. Doll, J. Chem. Phys. **93**, 2769 (1990).
[92] D. J. Chartrand (unpublished).
[93] M. A. Kmetic and R. J. Le Roy (unpublished).
[94] For the CMC(3B) case, confirmation of this conclusion is provided by the drop in the value of $\delta_{\mathrm{Ar-Ar}}$ at 18 K, seen in the middle segment of Fig. 5.
[95] T. S. McKay, D. J. Chartrand, and R. J. Le Roy (unpublished).
[96] Although this $8+3$ isomer is classically stable, the ground state for this cluster size is a monolayer.
[97] This behavior is confirmed by Ne–SF_6 and Ne–Ne radial distribution functions calculated for these runs.
[98] At 0.6 and 0.4 K, respectively, rapidly growing quantum effects required the use of 16 and 24 Fourier coefficients, to achieve convergence in the PIMC simulations, a fact which discouraged our extension of these runs to even lower temperatures.
[99] M. Lewerenz, B. Schilling, and J. P. Toennies, Chem. Phys. Lett. **206**, 381 (1993).